CHIN. PHYS. LETT. Vol. 36, No. 2 (2019) 025201

Successive Picket Drive for Mitigating the Ablative Richtmyer–Meshkov Instability *

Meng Li(李蒙)[1**], Wen-Hua Ye(叶文华)[1,2**]

[1]*Institute of Applied Physics and Computational Mathematics, Beijing 100094*
[2]*Center for Applied Physics and Technology, HEDPS, Peking University, Beijing 100871*

(Received 14 September 2018)

The ablative Richtmyer–Meshkov instability (ARMI) is crucial to the successful ignition implosion of the inertial confinement fusion (ICF) because of its action as the seed of the Rayleigh–Taylor instability. In usual ICF implosions, the first shock driven by various foots of the pulses plays a central role in the ARMI growth. We propose a new scheme for refraining from ARMI with a pulse of successive pickets. With the successive-picket pulse design, a rippled capsule surface is compressed by three successive shocks with sequentially strengthening intensities and ablated stabilization, and the ablative Richtmyer–Meshkov growth is mitigated quite effectively. Our numerical simulations and theoretical analyses identify the validity of this scheme.

PACS: 52.57.Fg, 52.57.−z, 47.20.−k, 52.50.Lp DOI: 10.1088/0256-307X/36/2/025201

The Rayleigh–Taylor instability (RTI) and the Richtmyer–Meshkov instability (RMI) play important roles in ICF and many other physical phenomena.[1,2] With the ablation driven by laser beams or x-rays in ICF, the ablative Rayleigh–Taylor instability (ARTI) and ARMI differ from the classical ones. On account of ARMI, any perturbation from the outer surface of a capsule would grow right away and be amplified by the followed ARTI during the acceleration phase of the implosion, and it will then feed through the shell to the inner deuterium-tritium (DT) ice layer and even break up the imploding shell during the deceleration phase. Thus, the capsule must be designed to keep the growth of these instabilities at an acceptable level to prevent them from endangering ignition of the capsule.

On the path to the capsule ignition using indirect drive (ID), designs and experiments have achieved significant progress. Initially, most attentions were paid to low foot (LF) drive. The experiments conducted on the National Ignition Facility (NIF) have achieved peak implosion velocity about 350 km/s, and the areal density of the DT fuel about 1.3 g/cm^2. Unfortunately, only $\sim 10^{14}$ neutrons were achieved, which is far below the goal of ignition.[3,4] Further experiments indicated that there was a high degree of ablator mix into the DT fuel due to high instability growth at the ablation front.[5,6] Then, experiments with the high foot (HF) drive increased neutron yields up to 10^{16}. High neutron yields in HF implosion are attributed to growth mitigation of the ARMI and the followed ARTI at the ablation front. Compared to the LF pulse, the mitigation is due to a much higher picket and a higher foot plateau of the HF pulse. Although the HF implosion has high stabilization at the ablation front, the high adiabat of DT fuel sacrifices high DT compression.[7] Therefore, the adiabat shaping (AS)[8−14] implosion is performed as a trade-off between compression and stability, in which high DT compression has been obtained.[4,15−17] However, the implosion stability still needs to be improved further.

According to hydrodynamic instability growth of the perturbation, the ICF implosion can be divided to the ARMI phase, the acceleration ARTI phase and the deceleration ARTI phase. Instability growth of the acceleration phase can be controlled by the HF and AS design with the high picket of the prepulse for the mitigation of ARMI growth.[18−20] Other attempts to suppress the ARTI are also on the way: the hybrid-drive ignition scheme is proposed to suppress implosion asymmetry and instabilities with indirect drive combined with direct drive,[21] and the decompression-recompression scheme is suggested to inhibit ARTI in the deceleration phase with the main pulse optimization.[22,23]

No matter whether the LF drive or the HF drive is employed, the first shock has the largest contribution to the DT fuel adiabat, which dominantly determines the density profile of the shell. Thus, the first shock drives the ARMI that seeds for subsequent hydrodynamic instability of the implosion. Hence, the seed from the ARMI during the prepulse, especially during the period of the first shock, is one of most important issues for the ID implosion and ignition, and should be investigated in depth. For example, with the AS pulse or the HF pulse, when a rippled capsule surface is radiated by the high picket, the strong first shock is formed quickly and runs ahead of the ablation front and to perturb the capsule interior, which become seeds of the following ARTI.[17,19,20]

In this Letter, we first propose a new pulse shape with successive pickets (SPs) to reduce the ARTI seeds

*Supported by the National Natural Science Foundation of China under Grant Nos 11675026, 11875091 and 11575034.
**Corresponding author. Email: li_meng@iapcm.ac.cn; ye_wenhua@iapcm.ac.cn
© 2019 Chinese Physical Society and IOP Publishing Ltd

during the early stage of the ID prepulse drive, which can compromise stability well with compression of the implosion.

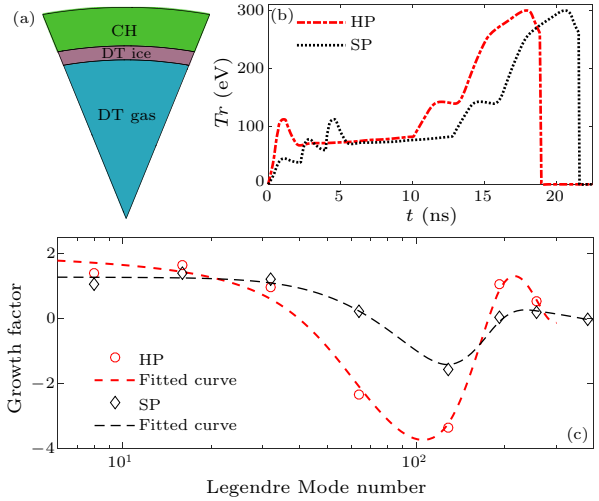

Fig. 1. (a) Sketch of the capsule, (b) radiation drives, and (c) ablation front GF spectra.

The cryogenic DT fusion capsule (Fig. 1(a)) is used in our numerical simulations. The capsule contains a 210-μm-thick CH ablator with density of 1.0 g/cm^3, an 80-μm-thick DT ice layer with density of 0.25 g/cm^3, and a DT-gas-filled cavity with a radius of 907 μm and density of 0.3 mg/cm^3. One-dimensional (1D) and two-dimensional (2D) single-mode perturbation simulations are performed with the radiation hydrodynamic code LARED-S.[24] The LARED-S code has been widely used in the study of ICF hydrodynamics instabilities.[21–27] It is a multidimensional massively parallel Eulerian code employing multi-group diffusion radiation transport, flux-limited Spitzer–Harm thermal conduction for electron and ion. With the fifth-order accurate WENO scheme, the 2D simulations mostly use 2000 × 40 zones with a domain width of one full wavelength along θ direction.

The drives of the SP pulse and the high picket (HP) pulse are plotted in Fig. 1(b). Both pulses have a peak temperature of 300 eV, and the troughs are kept at a relatively low level. By comparison, the sole HP pulse is presented with a red solid line and the SP pulse with a black dotted line. The only difference between them is that the sole high picket is replaced with three successive climbing up pickets. The shapes of the last SP picket and of the sole high picket are identical.

The growth factor (GF) is defined by the ratio of the ablation front amplitude of given mode at a time to its initial amplitude. The RM growth factors are shown schematically in Fig. 1(c), the initial sinusoidally perturbed amplitudes are all 0.5 μm for comparison. The GFs of the SP case (the black symbols and line) are evidently less than those of the HP case (the red symbols and line), especially at the bottom of negative lobes near Legendre mode 100. These small lobes will be amplified during the following acceleration phase of the imploding capsule. It has been found that the negative lobe threatens the capsule ignition.[15,28,29] Certainly the implosion stability benefits from the squeezing negative lobe.

The perturbation amplitudes of mode numbers 16 and 64 on the ablation front are both quite larger for the HP pulse than for the SP pulse (in Fig. 2(a)), these two selected modes are more sensitive for robustness of the hot spot surface and the ablation front, respectively. The overall oscillation frequencies of either of the two modes are close to each other. Via simulations with 40 and 220 grids (dash-dotted lines and dotted lines) in θ direction, the convergence of their numerical resolution is also identified in Fig. 2(a). Both of the perturbation amplitudes of the SP pulse (black lines and cyan lines) fade down during the first picket session, and then they dive downwards quickly and return to a platform during the second session. With the launch of the third picket, the perturbation amplitudes jump to a high level. In fact, they grow similar to that of the high picket in the HP case, but with a smaller increase. The shrinking oscillation amplitudes of the SP pulse are rooted in mitigations of the three pickets, especially the first picket.

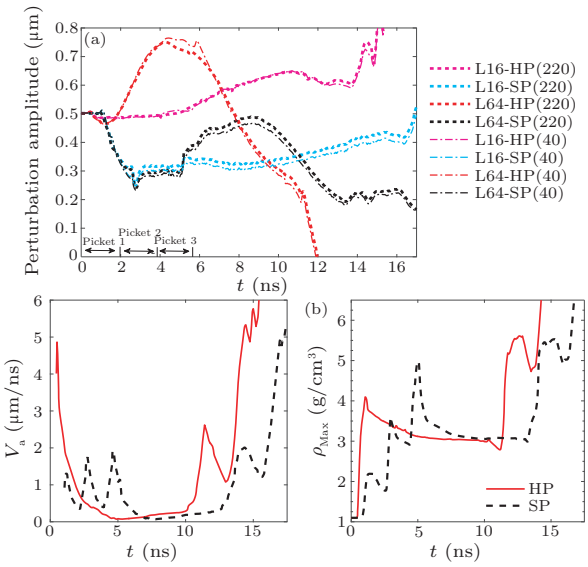

Fig. 2. Evolutions of (a) perturbation amplitudes of mode numbers 16 and 64 on the ablation front and (b) V_a, ρ_{Max}.

In the SP case, three sequentially strengthening shocks are generated, and the three shocks coalesce into one strong shock which is close to the shock driven by the sole high picket in the HP case. In Fig. 2(b), evolutions of the ablation velocity (V_a), and the peak density of the shell (ρ_{Max}) for the two pulses are compared. The two ablation velocities evolve quite different, the former grows very high almost immediately, the latter fluctuates at a lower level during the three pickets. The trajectories of ρ_{Max} indicate that the three compression ratios of the SP pulse at the early

stage are lower than the compression ratio of the HP pulse, especially the first shock compression ratio. Neglecting the early stage, the evolutions of V_a and ρ_{Max} in the HP and SP cases are close to each other—the behaviors of the latter are just postponed by about 3.5 ns.

Recall the formula of the perturbation amplitude on the ablation front[18]

$$\frac{\eta_a(k,t)}{\eta_0} = \frac{\eta_a^{cl}(k,t)}{\eta_0} - 1 + C_{(0)} - C_t k c_s t + \eta_{usu}(k,t) + \eta_\nu(k,t), \quad (1)$$

where $k = L/R$ is the wave number, L is the Legendre mode number, R is the capsule outer radius, c_s is the sound speed, and η_a^{cl} is the perturbation evolution in the absence of mass ablation. The usual ablative RMI and vorticity convection terms are[19]

$$\begin{aligned}\eta_{usu}(k,t) &= e^{-2kV_a t}(\alpha_0\cos(\omega t) + \beta_0 \sin(\omega t)),\\ \eta_\nu(k,t) &\approx -f(C)\frac{c_s}{V_{bl}}\left\{e^{kV_a t}\left[1 - \frac{1}{1+e^{-3(kV_a t - 0.55)}}\right] + \frac{\sin(\sqrt{3}kV_a t)}{2\sqrt{kV_a t}}\right\}\\ &= \eta_{\Omega 1} + \eta_{\Omega 2},\\ V_{bl} &\approx V_a/(2.4kL_0/\nu)^{1/\nu}, \end{aligned} \quad (2)$$

where V_a and V_{bl} are the ablation and blow-off velocities, respectively, oscillatory frequency $\omega = k\sqrt{V_a V_{bl}}$, and C is the first shock compression ratio. The coefficients $C_{(0)}$, C_t, α_0 and β_0 are defined in Ref. [18].

The oscillation amplitude on the ablation front is closely related to the mode number and the ablation velocity. For a single mode, the oscillation amplitude is damped and polarizes. A low-mode perturbation experiences positive growth and a high-mode one undergoes phase reversal, just like the behaviors of mode 16 and 64.

When $kV_a t \ll 1$, $|\eta_{\Omega 1}| \gg |\eta_{\Omega 2}|$, the stabilization depends on the contribution of the vorticity convection term $\eta_{\Omega 1}$. For a lower picket, the shock intensity and the ablation velocity are reduced, and the duration that satisfies $kV_a t \ll 1$ becomes longer, so that the $\eta_{\Omega 1}$ term plays a more active role. Meanwhile, for the RMI without mass ablation, the growth rate of RMI decreases relative to the Mach number of the incident shock.[30] Vorticity is considered as important quantity to determine the RMI growth rate in the linear stage. When the shock is weaker, the stored vorticity intensity is lower,[31] and then the RMI growth decreases. Hence, the η_a^{cl} term grows slowly due to the relatively weak shock. On the whole, the SP pulse leads to a considerable mitigation of the perturbation amplitude.

The density contour diagrams of mode 64 are shown in Fig. 3, and they located at the beginning of shell acceleration and the moments of peak implosion velocity. All the black dash-dotted curves represent the interface between CH and DT ice. The green, magenta and white curves in Fig. 3(a) represent isolines of 0.5, 1.5 and 2.5 g/cm^3, respectively. The green and magenta curves in Fig. 3(b), represent isolines of 5.0 and 15.0 g/cm^3, respectively. At the two moments, the gap between the SP and HP cases widens out. The instability growth mitigations of the SP pulse emerge more significantly at the moment of peak implosion velocity. It is of note that the implosion and ignition process go on smoothly and achieve a yield-over-clean (YoC) of about 0.5 in the SP case, the HP's fusion reaction is truncated due to lack of confinement of the breakup shell. Evidence of the advantage of a lower foot radiation temperature was laid out by MacPhee *et al.*[32] A long toe (∼100 eV) reduces perturbation of the fill tube embedded in the capsule. Further benefits of a lower toe can be expected.

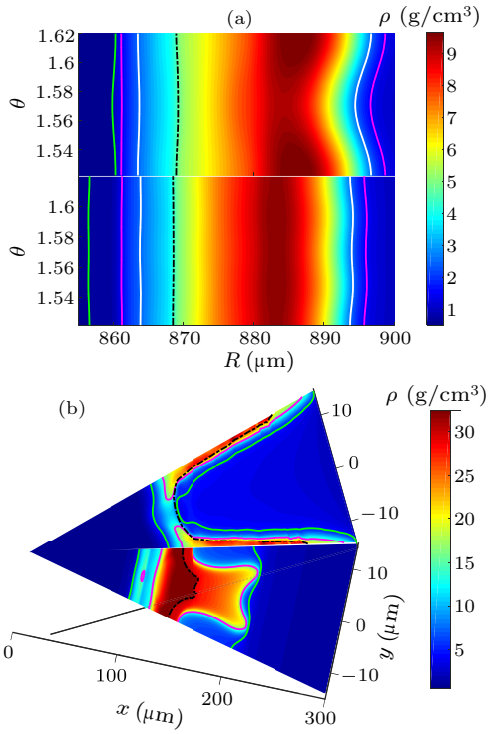

Fig. 3. Density contour diagrams of mode 64 in the HP and SP cases (a) at the beginning of acceleration phase and (b) at the time of peak implosive velocity.

In summary, the ARMI growth can be regarded as producing, relaxing and eradicating vortices. This can be significantly reduced with carefully tailored shocks when it is not sufficiently developed during the early linear stage. With our new SP pulse design, the ARMI growth is reduced considerably, meanwhile compression of the capsule shell is increased. Implosion performance is improved obviously in 2D simulations by the SP design due to the reduced seeds of the ARTI during the acceleration stage. Therefore, the SP pulse scheme enriches the hydrodynamic instability control strategy for the ignition capsule design. This deserves

to be widely used in direct and indirect drive ICF implosion.

References

[1] Lindl J D 1998 *Inertial Confinement Fusion* (Springer: New York)
Atzeni S and Meyer-ter-Vehn J 2004 *The Physics of Inertial Fusion* (Oxford: Clarendon Press)
[2] Zhou Y 2017 *Phys. Rep.* **720** 1
Zhou Y 2017 *Phys. Rep.* **723** 1
[3] Edwards M J, Patel P K, Lindl J D et al 2013 *Phys. Plasmas* **20** 070501
[4] Smalyuk V A, Goncharov V N, Anderson K S et al 2007 *Phys. Plasmas* **14** 032702
[5] Ma T, Patel P K, Izumi N, Springer P T et al 2013 *Phys. Rev. Lett.* **111** 085004
[6] Regan S P, Epstein R, Hammel B A et al 2012 *Phys. Plasmas* **19** 056307
[7] Hurricane O A, Callahan D A, Casey D T et al 2014 *Nature* **506** 343
[8] Gardner J H, Bodner S E and Dahlburg J P 1991 *Phys. Fluids B* **3** 1070
[9] Velikovich A L, Cochran F L and Davis J 1996 *Phys. Rev. Lett.* **77** 853
[10] Bodner S E, Colombant D G, Gardner J H et al 1998 *Phys. Plasmas* **5** 1901
[11] Goncharov V N, Knauer J P, McKenty P W et al 2003 *Phys. Plasmas* **10** 1906
[12] Anderson K and Betti R 2003 *Phys. Plasmas* **10** 4448
[13] Betti R, Anderson K, Knauer J et al 2005 *Phys. Plasmas* **12** 042703
[14] Campbell E M, Goncharov V N, Sangster T C et al 2017 *MRE* **2** 37
[15] Clark D S, Milovich J L, Hinkel D E et al 2014 *Phys. Plasmas* **21** 112705
[16] Peterson J L, Berzak Hopkins L F, Jones O S and Clark D S 2015 *Phys. Rev. E* **91** 031101
[17] Robey H F, Smalyuk V A, Milovich J L et al 2016 *Phys. Plasmas* **23** 056303
[18] Goncharov V N, Gotchev O V, Vianello E et al 2006 *Phys. Plasmas* **13** 012702
[19] Peterson J L, Clark D S, Masse L P et al 2014 *Phys. Plasmas* **21** 092710
[20] Landen O L, Baker K L, Clark D S et al 2016 *J. Phys.: Conf. Ser.* **717** 012034
[21] He X T, Li J W, Fan Z F et al 2016 *Phys. Plasmas* **23** 082706
[22] Wang L F, Ye W H, Wu J F et al 2016 *Phys. Plasmas* **23** 052713
[23] Wang L F, Ye W H, Wu J F et al 2016 *Phys. Plasmas* **23** 122702
[24] He X T and Zhang W Y 2007 *Eur. Phys. J. D* **44** 227
[25] Ye W H, Zhang W Y and Chen G N 1998 *High Power Laser Part. Beams* **10** 403 (in Chinese)
[26] Ye W H, Zhang W Y and He X T 2002 *Phys. Rev. E* **65** 57401
[27] Wang L F, Xue C, Ye W H and Li Y J 2009 *Phys. Plasmas* **16** 112104
[28] Clark D S, Haan S W, Hammel B A et al 2010 *Phys. Plasmas* **17** 052703
[29] Hammel B A, Haan S W, Clark D S et al 2010 *High Energy Density Phys.* **6** 171
[30] Holmos R L, Dimonte G, Fryxell B et al 1999 *J. Fluid Mech.* **389** 55
[31] Wouchuk J G and Cobos-Campos F 2017 *Plasma Phys. Control. Fusion* **59** 014033
[32] MacPhee A G, Casey D T, Clark D S et al 2017 *Phys. Rev. E* **95** 031204